Microstructure refinement and mechanical properties improvement of Al-Si-Fe alloys by hot extrusion using a specially designed high-strain die

Shino Sakow[1], Toko Tokunaga[2*], Munekazu Ohno[2], Kiyotaka Matsuura[2]

[1] formerly Graduate School of Engineering at Hokkaido University, Kita 13 Nishi 8, Kita-ku, Sapporo, Hokkaido 060-8628, Japan, presently Caterpillar Japan LLC, Shimizu 1106-4, Uozumi-cho, Akashi, Hyogo 674-8686, Japan

[2] Faculty of Engineering, Hokkaido University, Kita 13 Nishi 8, Kita-ku, Sapporo, Hokkaido 060-8628, Japan

*corresponding author: tokunaga@eng.hokudai.ac.jp

Abstract

A heteromorphic extrusion die with right-angle corners in the die hole was designed in this study to give a high local strain to the extrudate metal during hot extrusion of Al-Si-Fe alloys, and the strain distribution in the extrudate metal was evaluated using the finite element method. It was demonstrated that the change in metal flow direction at the right-angle corners is effective for generating high strain in the extrudate metal and refining brittle inclusion particles such as primary $Al_9Si_2Fe_2$ (β phase) particles and eutectic Si particles. The refinement of these particles led to significant improvements in tensile elongation and plastic deformability in cold rolling of the alloys.

Keywords
Al-Si alloy, intermetallic phase, heteromorphic die extrusion, elongation

1. Introduction

In recent years, Al alloys have been increasingly utilized for parts of vehicles to reduce weight of vehicles, which contributes to improvement of fuel efficiency and reduction in CO_2 emission. Particularly, Al-Si alloys are widely used for automobile parts because of their excellent castability, high wear resistance and low thermal expansion coefficient (G. Ham, et al., 2017). Moreover, the Al-Si alloys are mainly produced from recycled Al scrap, which reduces production energy by 95% compared with the production of the alloys from the primary metal (S.K. Das, et al., 2010). Thus, recycled Al-Si alloys are important industrial materials from ecological and economical points of view.

The recycled Al-Si alloys contain many impurity elements derived from scrap, e.g., Fe, Mn, Cu and Zn. Among these elements, Fe is particularly harmful, because it forms coarse plate-like intermetallic compound particles, $Al_9Si_2Fe_2$ (β phase), during solidification. The β phase deteriorates mechanical properties of the Al-Si alloys because it is extremely brittle, and it can be a crack initiation site (L. Fang, et al., 2011). Thus, as the number of recycling times increases, the Fe concentration in the recycled Al scrap increases and the quality of the industrial Al-Si alloys decreases due to the increase of the harmful effects of the β phase. In industry, the Fe concentration is usually reduced by the addition of pure Al ingots to the molten recycled Al alloys, which wastes the ecological and economical advantages of recycling of Al. If the recycled Al alloys could be used as they are without diluting with pure Al, it would be industrially advantageous. The use of recycled Al alloys in industry without dilution with pure Al will be possible when the harmful effects of the β phase are mitigated. Several methods have been proposed and developed to eliminate the harmful effect of the β phase, e.g., powder metallurgy (F. Prusa, et al., 2015), addition of inoculant elements (Y. Cai, et al., 2011), and ultrasonic vibration to the molten alloy (W. Khalifa, et al., 2010). Although these techniques are effective in refining the β phase particles, they have some problems such as formation of other brittle particles or a limited narrow range of applicable production conditions.

In this study, we propose the use of a specially designed extrusion die to reduce the β particle size dramatically to eliminate the harmful effect of the β particles, and the reuse of recycled Al-Si-Fe alloys with refined β particles as wrought materials instead of cast materials. This paper focuses on the feasibility of the β particle refining process and the possibility of the reuse of the recycled Al-Si-Fe alloys as wrought materials.

2. Experimental procedure

2.1 Hot extrusion

Al-12mass%Si-xFe (x = 2, 4 mass%) alloys were used as model materials of recycled Al-Si alloys in this study. Liquid alloys made of commercial pure Al (99.99% purity), Al-25mass%Si alloy and Fe powder (99.99% purity) were cast into a cylindrical ingot having a diameter of 44 mm and a height of 140 mm, and the ingot was used as a billet for extrusion after removing the top part of 40 mm in height including the shrinkage cavity.

The extrusion die used in this study is illustrated in Fig. 1. The die was designed by the present authors and named as a heteromorphic die, which consists of a strain-giving die and a shape-giving die. They were set up in the bottom of the extrusion container as shown in Fig. 1 (a). The strain-giving die has four holes with a diameter of 6.5 mm on the side surface and a hole with a diameter of 13 mm on the bottom surface, as illustrated in Fig. 1 (b). This die gives a large shear strain to the billet metal by forcibly changing the metal flow direction at a right angle when the metal goes into the holes on the side surface of the die and when it goes out from the other hole on the bottom surface of the die. On the other hand, the shape-giving die has a square hole with a side length of 11.5 mm, as illustrated in Fig. 1 (c), and finally gives a shape to the metal. Between the two dies, a ring-shaped spacer was placed to fix the position of each die and to make a space containing the metal coming down from the strain-giving die hole and going down into the shape-giving die hole, as shown in Fig. 1 (a). The outer and inner diameters and height of the spacer were 44, 14 and 10 mm, respectively. In the space inside the ring-shaped spacer, a cylindrical alloy block having the same chemical composition as that of the billet was placed before extrusion in advance, which played a role of a dummy. The container was placed in an electric heater, and the heteromorphic die, the billet and the ram were placed in this order from the bottom of the container. Then, the load was applied to the ram to extrude the billet. The billet metal first entered the strain-giving die from the four horizontal holes, and emerged from the vertical hole on the bottom, and then it filled the inside of the spacer pushing the dummy towards the shape-giving die hole and finally it was extruded downwards in the form of a square bar. The extrusion temperature was set at 450°C, and the extrusion ratio was 13, calculated by dividing the cross-sectional area of the billet by the cross-sectional area of the extruded square bar.

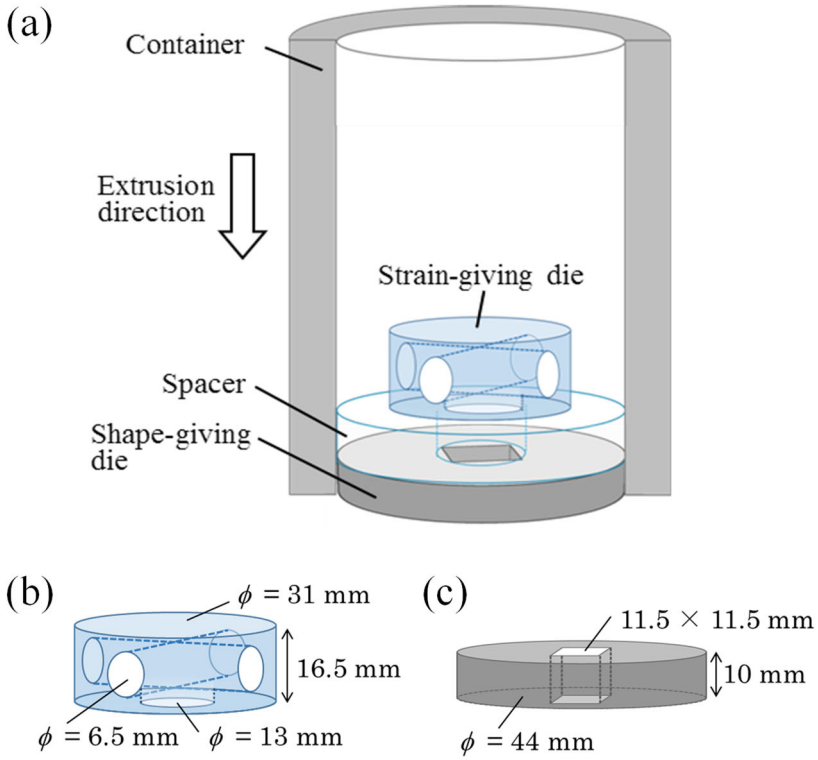

Fig. 1 Schematic drawing of heteromorphic die extrusion; (a) the overall setup, (b) strain-giving die and (c) shape-giving die.

2.2 Cold rolling

From the extruded square bar, a cuboid sample having a thickness and a width of 10.5 mm and a length of 50 mm was cut out. The longitudinal direction of the cuboid sample was the same as the extrusion direction. The sample was rolled at room temperature with a rolling reduction of 77%. The final thickness of the rolled sample was 2.4 mm. The rolling was carried out in two passes, 55% reduction in the first pass and the same with the second pass. The roll diameter was 160 mm, and the roll rotational speed was 11.9 rpm. As a comparison, a similar cold rolling was also conducted on the billet without extrusion. The rolling conditions for the billet were equal to those for the extruded bar.

2.3 Microstructure observation

Microstructure observation was conducted for all samples obtained from the above-mentioned experiments. Each sample was polished with emery paper up to #2000 and then finished with an alumina suspension with a particle diameter of 100 nm. The polished samples were observed by an optical microscope. Also, Electron BackScatter Diffraction (EBSD) technique was used to observe the distribution of the inclusion particles and the grain structure of the Al matrix phase.

2.4 Tensile test

Tensile specimens were cut from the billet, the extruded bar and the rolled sheet by using a wire electric discharge machine. Tensile specimens cut out from the cold rolled sheet were heat-treated at 200°C for 1 h for strain relaxation. Fig. 2 shows a schematic diagram of the tensile test specimen. The tensile specimens without extrusion were taken from the center of the ingot. The tensile specimens for the extruded bar and the rolled sheet were taken so that the tensile direction corresponded to the extrusion and the rolling directions. The tensile tests were conducted at room temperature at a strain rate of 1.0×10^{-3} s^{-1}. After the tests, fracture surfaces of each sample were observed using a Scanning Electron Microscope (SEM).

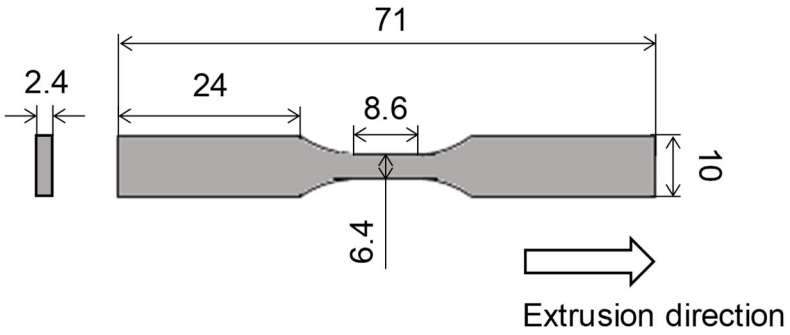

Fig. 2 Schematic diagram of the tensile test specimen (dimensions in mm).

3 Finite element analysis

To investigate the effect of the heteromorphic die extrusion on the microstructure refinement, effective strain generating in the billet metal during the heteromorphic die extrusion was simulated by using a commercial Finite Element (FE) software, Forge 2011. To simplify the simulation, only the behavior of the metal passing through the strain-giving die was focused. For comparison, an extrusion process with a conventional die was also simulated. Fig. 3 shows the developed geometries of (a) the heteromorphic die extrusion and (b) the conventional die extrusion. In this simulation, a two-dimensional axisymmetric model was developed, taking into account the symmetry of the extrusion equipment. For simplicity, the die is incorporated in part of the container in the model geometries as shown in Fig. 3. To avoid an error originating from mesh distortion problem, the ram was designed larger than the real size and it partially penetrated the container. The shape and size of the die hole of the conventional die extrusion was the same as those of the shape-giving die in the heteromorphic die extrusion. In the simulation process, the billet was extruded from the die hole by moving the ram downward at a speed of 0.2 mm/s same as that in real experiment. The FE code was based on the Norton-Hoff viscoplastic flow rule (J.-L. Chenot and M. Bellet, 1992):

$$\boldsymbol{s} = 2K\left(\sqrt{3}\dot{\bar{\varepsilon}}\right)^{m-1}\dot{\boldsymbol{\varepsilon}} \quad (1)$$

where $\boldsymbol{s}$ is the deviatoric stress tensor, K is the material consistency, m is the strain rate sensitivity, $\dot{\boldsymbol{\varepsilon}}$ is the strain rate tensor and $\dot{\bar{\varepsilon}}$ is the effective strain rate, which is described as

$$\dot{\bar{\varepsilon}} = \left(\frac{2}{3}\sum_{i,j}\dot{\varepsilon}_{ij}^{2}\right)^{\frac{1}{2}} . \quad (2)$$

A flow stress model described in the following Eq. (3) was selected from Forge database which represents an Al-12Si-1Cu-1Mg-1Ni (mass%) alloy. Although the composition of this alloy is not exactly the same as that of the alloy used in the present experiment, there will not be any problem because the present simulation is performed to compare the strain distribution in the extruded alloy between the heteromorphic die extrusion and the conventional die extrusion. The flow stress model is described by Hansel-Spittel law (M.El. Mehtedi, et al., 2014) as below:

$$\sigma = 488.57981\exp(-0.00537T)\varepsilon^{0.03987}\dot{\varepsilon}^{0.12904}\exp\left(\frac{-0.00431}{\varepsilon}\right). \quad (3)$$

This flow stress model can be used in a temperature range from 250 to 550ºC, which fully covers the present extrusion temperature of 450ºC. The geometry dimensions of the extrusion container and the dies of the model were same as those in the real experiment.

The meshes of the die and the container were homogeneous, while the mesh of the billet was inhomogeneous, and its size was set finer in positions where the billet particularly undergoes severer plastic deformation as seen as a dark region in Billet in Fig. 3.

It was assumed that at all the interfaces, the friction behavior followed the Coulomb limited Tresca law which is described as below:

$$\tau = \mu\sigma_n\frac{\Delta \boldsymbol{v}}{\Delta u} \text{ if } \mu\sigma_n < \bar{m}\frac{\sigma_0}{\sqrt{3}} \quad (4)$$

$$\tau = \bar{m}\frac{\sigma_0}{\sqrt{3}}\frac{\Delta \boldsymbol{v}}{\Delta u} \quad \text{if} \quad \mu\sigma_n > \bar{m}\frac{\sigma_0}{\sqrt{3}} \quad (5)$$

where τ is the shear stress, μ is the Coulomb coefficient, σ_n is the normal stress vector, $\bar{m}$ is the shear friction coefficient and $\Delta\boldsymbol{v}$ and Δu are the vector and scalar values of velocity difference between two solid materials. The friction coefficients μ and $\bar{m}$ were set at 0.80 and 1.6 at the container/billet interfaces, while they were set at 0.075 and 0.15 at the die/billet or the billet/ram interfaces. The extrusion temperature was set at 450ºC. For the sake of simplicity, the container, the die and the ram were considered as rigid and the friction coefficients were set at constant during the process.

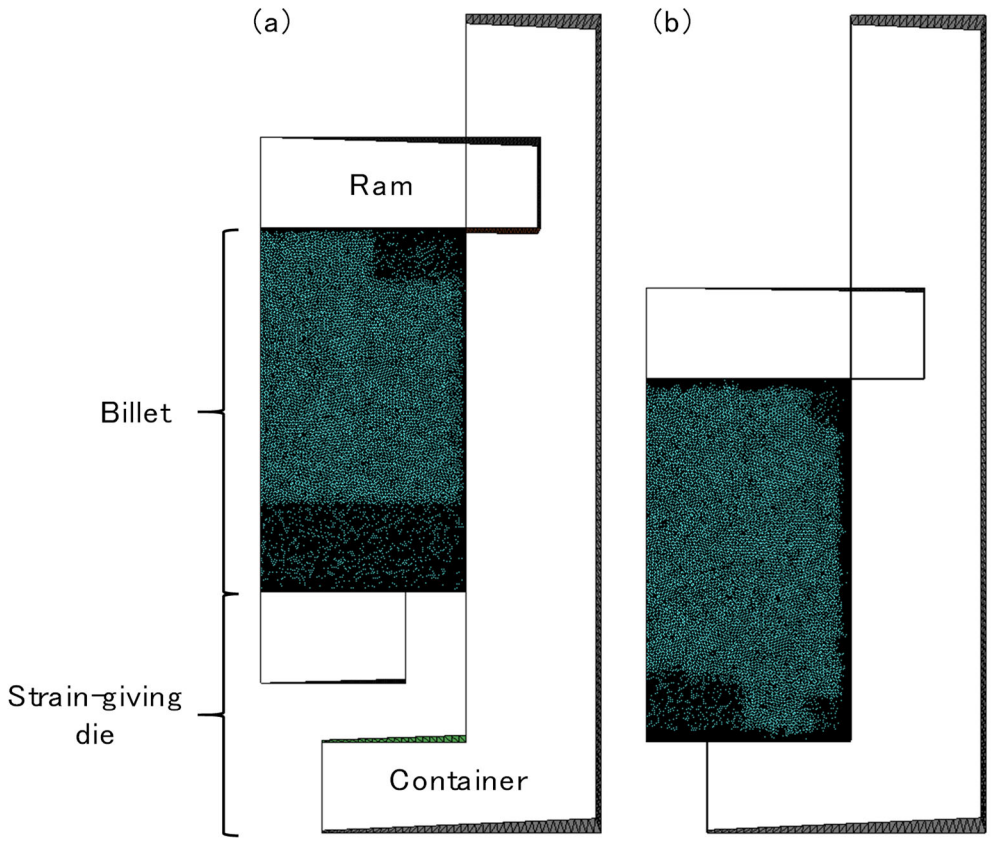

Fig. 3 The geometries of (a) the heteromorphic die extrusion and (b) the conventional die extrusion.

4. Results and discussion

4.1 Microstructure

Fig. 4 shows the microstructure images of the Al-12Si-2Fe alloy billet (a) before and (b) after the heteromorphic die extrusion, and the Al-12Si-4Fe alloy billet (c) before and (d) after the heteromorphic die extrusion. The white arrows in the figures indicate primary $Al_9Si_2Fe_2$ (β phase). The extrusion direction is perpendicular to the paper surface. The as-cast microstructure consists of huge β phase particles and coarse eutectic Si particles, as seen in Figs. 4 (a) and (c). The amount and the size of the β phase particles are significantly larger in the Al-12Si-4Fe alloy (Fig. 4 (c)) compared with the ones in the Al-12Si-2Fe alloy. Both the β phase and the eutectic Si particles were broken into small pieces after the heteromorphic die extrusion, as seen in Figs. 4 (b) and (d).

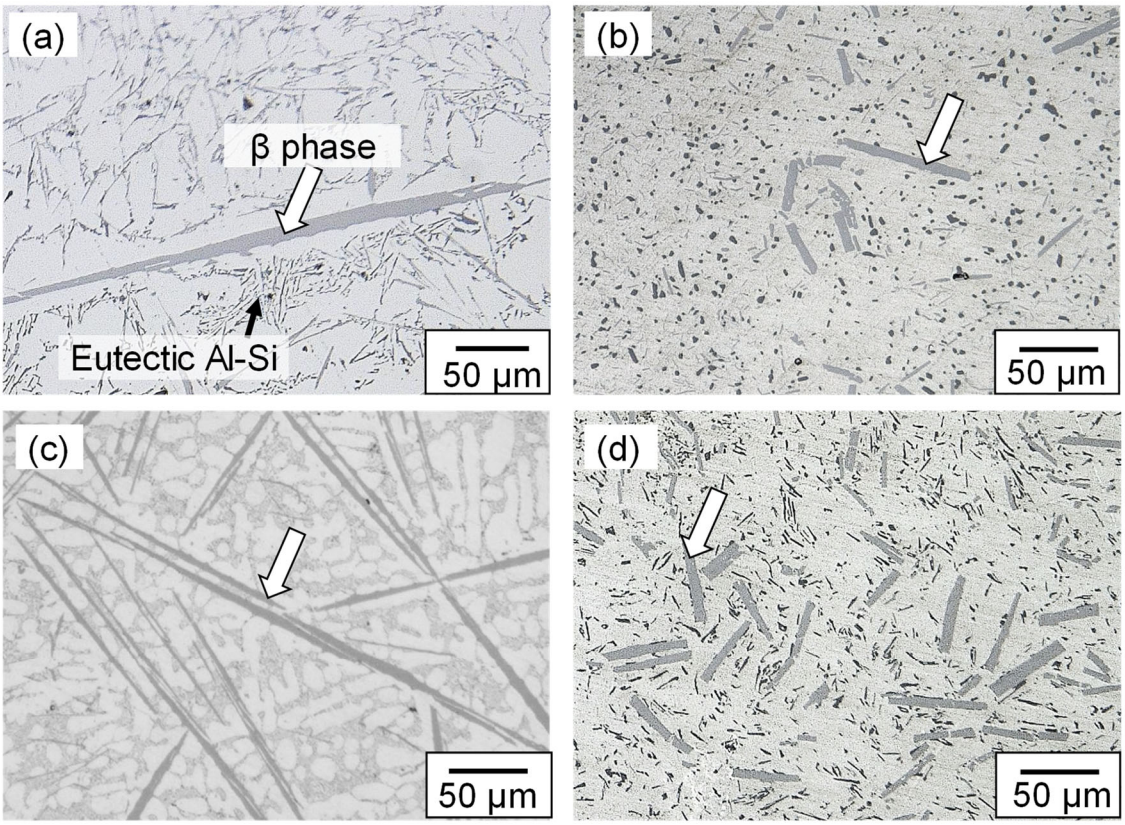

Fig. 4 Microstructures of (a) billet and (b) heteromorphic die extrudate containing 2 mass%Fe, and (c) billet and (d) heteromorphic die extrudate containing 4 mass%Fe. The white arrows in the figures indicate the β phase.

To observe the microstructure refinement process in detail, the extrusion was interrupted, and the billet was sectioned together with the die. Fig. 5 (a) shows a cross-section of the strain-giving die and a billet of the Al-12Si-4Fe alloy. Detailed microstructures of the alloy were observed in the four different positions indicated as (b) to (e) in Fig. 5 (a). Bold white arrows in each figure indicate the primary β phase particles. At a position in the container distant from the strain-giving die (Fig. 5 (b)), many coarse plate-like β phase particles are observed together with the dendrites of the Al-based solid solution and the eutectic Si particles in the interdendritic regions. Since the billet in this position had not undergone plastic deformation yet, the β phase particles and the dendrites have random orientations. However, as seen in Fig. 5 (c), when the billet metal reaches the gap between the container wall and the strain-giving die, their orientations become vertical and the β phase particles are broken down into small pieces although some particles are still huge and long. Next, when the metal enters the horizontal hole of the strain-giving die (Fig. 5 (d)), the orientation of the β phase particles also becomes horizontal and they are all broken into small pieces. Finally, the metal flow direction changes from horizontal to vertical when the metal reaches the vertical hole of the strain-giving die (Fig. 5 (e)). The area-equivalent diameters of the β phase particles were measured at the positions (b) to (e), and the average values at these positions were 20.6, 13.7, 12.8, and 12.0 μm, respectively. As a result, it was found that the most considerable refinement occurred at the position (c). However, focusing on the distribution of the β phase particles, it became more homogeneous when the metal flow changes its direction at the positions (d) and (e). It was suggested that the refinement and homogeneous distribution of the primary β phase and the eutectic Si particles were attributed to the large strain due to the heteromorphic die extrusion. To investigate the effect of the strain on the refinement and the homogeneous distribution more precisely, we performed a computer simulation of the plastic deformation of the billet during extrusion, as described in detail in the next section.

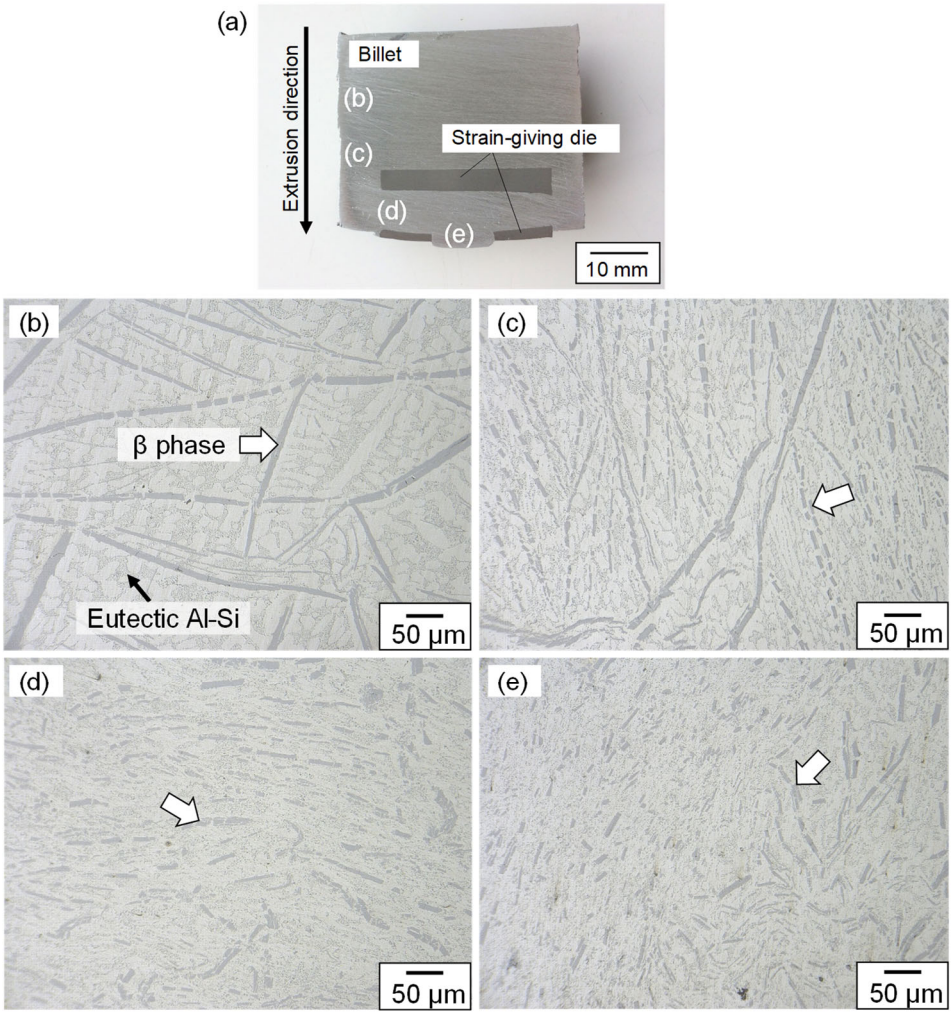

Fig. 5 (a) Cross section of strain-giving die and billet of Al-12mass%Si-4mass%Fe alloy. Figs (b) to (e): microstructures of the alloy in the positions indicated in (a). The white and black arrows indicate the β phase particles and the eutectic Si particles.

4.2 FE simulation of the heteromorphic die extrusion process

Fig. 6 illustrates the results of the simulation of effective strain distributions after the conventional die extrusion process (Figs. 6 (a) and (c)) and the heteromorphic die extrusion process (Figs. 6 (b) and (d)). It is clear from the results that the heteromorphic die extrusion can give much higher effective strain on the final extrudate. Table 1 shows the maximum and the minimum values of the effective strain obtained from the simulation after the both extrusion processes. The maximum effective strain of the heteromorphic die extrudate was about 50% higher than that of the conventional die extrudate. Moreover, Figs. 6 (b) and (d) clearly show that extremely high strain is generated in the gap between the container wall and the die (area indicated by an arrow A), at the corner near the entrance to the horizontal hole of the die (area indicated by an arrow B), and at the corner near the exit to the vertical hole of the die (area indicated by an arrow C). These three positions correspond to the positions (c), (d), and (e) in Fig. 5, where the primary β phase and the eutectic Si particles were refined and homogeneously distributed. Therefore, it is strongly suggested that the extremely high strain generated in the present heteromorphic die extrusion led to the refinement and the homogeneous distribution of the primary β phase and the eutectic Si particles.

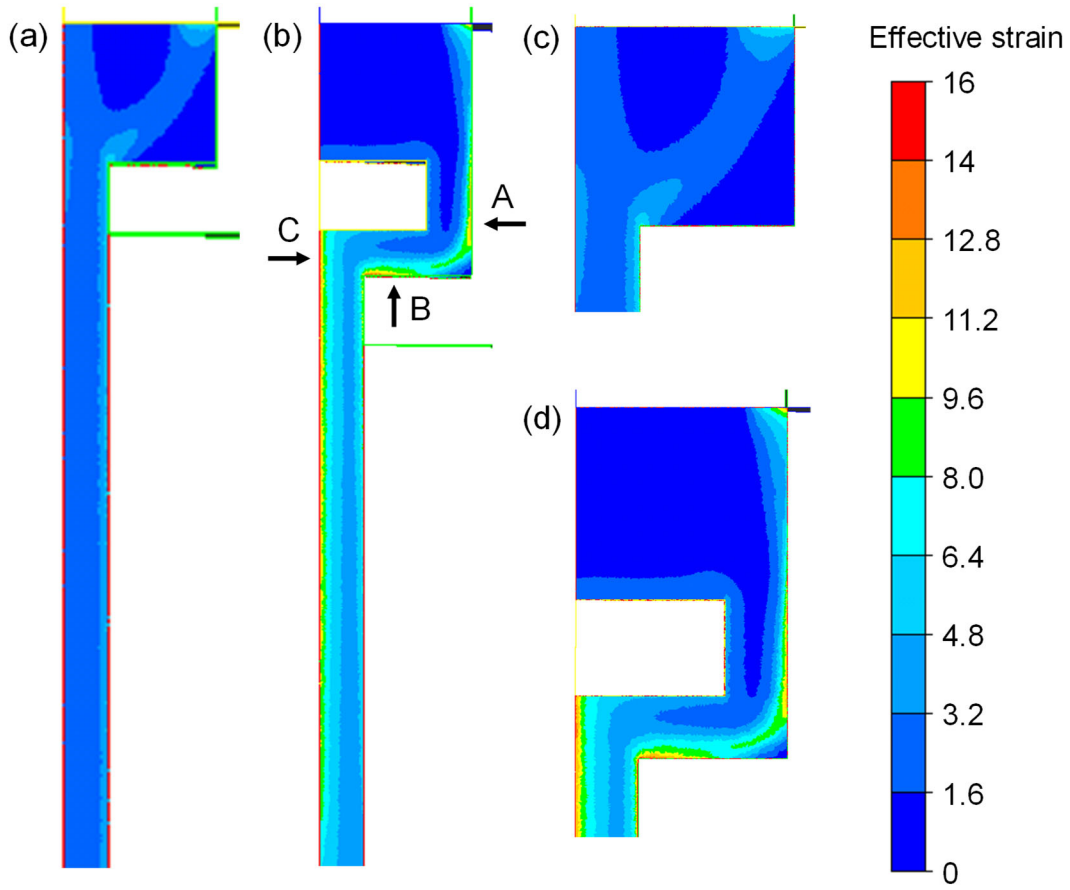

Fig. 6 Finite element simulation results of effective strain after (a) conventional die extrusion and (b) heteromorphic die extrusion processes. Figs. (c) and (d) represent enlargements of Figs (a) and (b), respectively.

Table 1 Effective strain values obtained from the simulation results after heteromorphic die and conventional die extrusion processes.

	maximum	minimum
Heteromorphic die extrusion	15.5	0.135
Conventional die extrusion	9.39	0.0464

4.3 Tensile tests

Fig. 7 shows the tensile test results of (a) the as-cast billet containing 2 mass%Fe, (b) the heteromorphic die extrudate containing 2 mass%Fe, (c) the as-cast billet containing 4 mass%Fe and (d) the heteromorphic die extrudate containing 4 mass%Fe. The as-cast billet specimens of (a) and (c) fractured with small elongations of 2 and 1%, respectively. However, the elongations dramatically increased to 43 and 22% when the billets were extruded using the heteromorphic die, as seen in (b) and (d). Also, strengths of the alloys were improved to 160 and 128 MPa in the alloys with 2 and 4 mass% of Fe, respectively. Therefore, the heteromorphic die extrusion can improve not only

elongation but also strength of the alloys. To investigate the reason for the dramatic improvement in the mechanical properties, fracture surfaces of the Al-12Si-4Fe alloy specimens were observed. Fig. 8 (a) shows the fracture surface of the as-cast billet specimen, revealing smooth surfaces of the β phase particles in the Al matrix. This is an evidence showing that the coarse plate-like β phase particles have a critical effect on the fracture and the deterioration in elongation of the specimen. In Fig. 8 (a), the surface of as-solidified dendrite arms can be also observed in cavities formed between the β phase particles. These cavities are considered as shrinkage holes caused by the coarse plate-like β phase particles blocking the melt supply into the cavity. On the other hand, as seen in Fig. 8 (b), the fracture surface of the heteromorphic die extrudate specimen is occupied mainly by the dark gray dimples of the Al matrix, indicating a ductile behavior of the fracture. Although smooth bright surfaces of the β phase particles can also be seen in Fig. 8 (b), their size is small and their distribution is homogeneous, compared with those in Fig. 8 (a). This fine and homogeneously-distributed β phase particles led to the improvement in elongation, and therefore, the heteromorphic die extrudates exhibited much higher strengths than the ones of the as-cast billet. Furthermore, since grains in the alloys were significantly refined by the heteromorphic die extrusion, it can be considered that grain refinement strengthening occurred. Consequently, it can be considered that the increase in elongation and strength shown in the stress-strain curves in Fig. 7 results from the refinement and the homogeneous distribution of the brittle particles of the primary β phase and the eutectic Si.

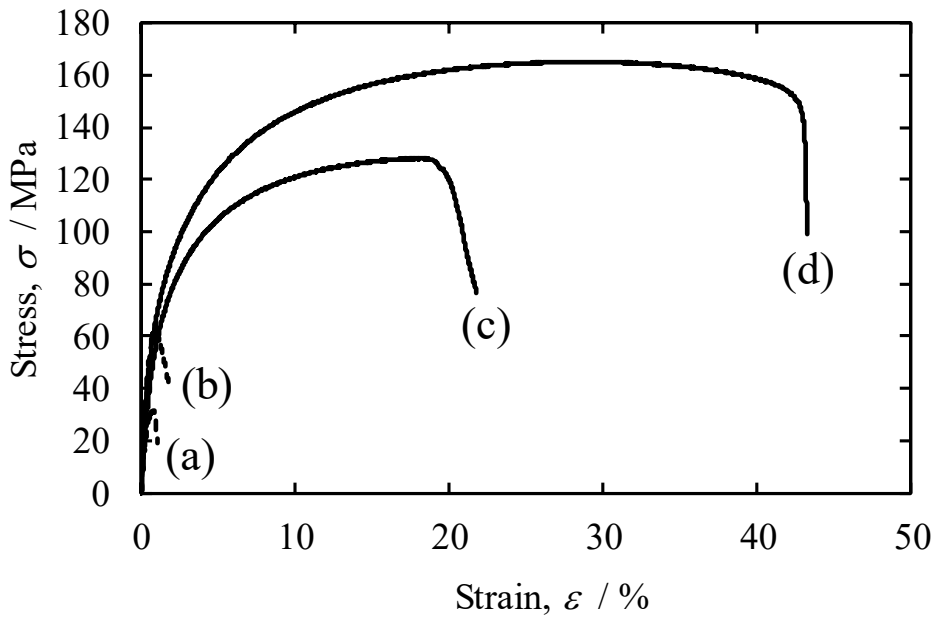

Fig. 7 Tensile test results of (a) as-cast billet containing 4 mass%Fe, (b) as-cast billet containing 2 mass%Fe, (c) heteromorphic die extrudate containing 4 mass%Fe, and (d) heteromorphic die extrudate containing 2 mass%Fe.

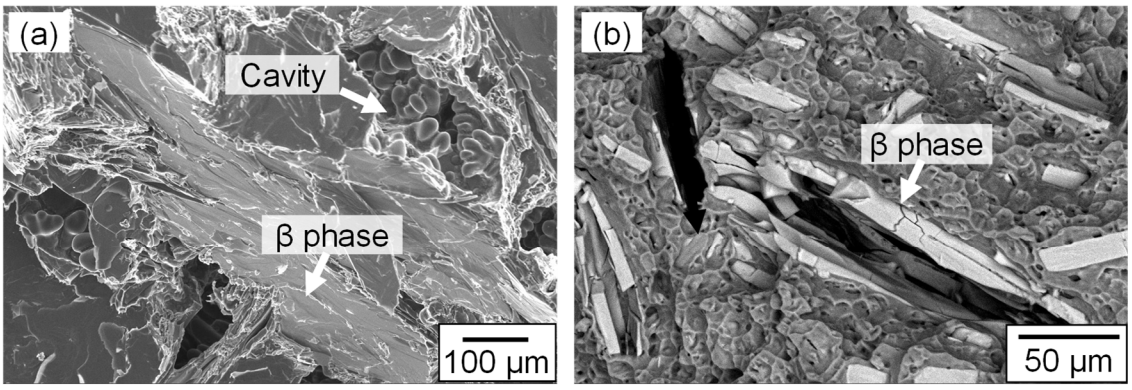

Fig. 8 Fracture surface of (a) the billet and (b) the heteromorphic die extrudate containing 4 mass%Fe.

To find an evidence of the above consideration, the relationship between the elongation and the size of the β phase particles in Al-12Si-*x*Fe (x = 0, 2, 4 (mass%)) alloys was investigated and the results are summarized in Fig. 9. The number written beside each plot in the figure shows the volume fraction (%) of the β phase particles. Although volume fraction of the β phase varies by each tensile specimen, there is a clear tendency of linear decrease in elongation with increasing size of the β phase particles. However, it is also seen in the figure that several plots with high volume fraction values deviate downward from the linear tendency. These results indicate that the elongation is affected not only by the size of the β phase particles but also by the volume fraction of the particles. To distinguish the effects of the diameter D (μm) and the volume fraction f_v (%) on the elongation ε_{max} (%), multiple regression analysis method was used, and the result is described as Eq. (6). The correlation coefficient R^2 for this analysis was 0.86 being notably high.

$$\varepsilon_{max} = 57.1 - 0.96\,D - 2.49\,f_v \qquad (6)$$

According to Eq. (6), the elongation decreases by approximately 1% as the diameter increases by 1 μm, and it decreases by approximately 2.5% as the volume fraction increases by 1%.

As described above, the present heteromorphic die extrusion dramatically increased the elongation of the Al-Si-Fe alloys, and it has been considered that the increase in elongation is attributed to the decreases in diameter and volume fraction of the β phase particles. However, it can also be considered that the grain size of the Al matrix or the size of the eutectic Si particle can also affect the elongation. To investigate the effect of the grain size of the Al matrix and the size of the eutectic Si particles, EBSD analysis was conducted. Fig. 10 shows the crystal orientation mapping obtained from the heteromorphic die extrudate of (a) Al-12Si-2Fe and (b) Al-12Si-4Fe alloys. The extrusion direction is transverse on the paper surface as indicated by an arrow (ED) in the figure. The EBSD analysis was

conducted with energy dispersive X-ray spectrometry analysis simultaneously to distinguish the Al matrix and the Si particles. Because Fig. 10 shows only the results of the Al matrix, the black regions in the figure represent the Si particles. From these mappings, there are no significant difference in size of the Si particles between Figs. 10 (a) and (b). Also, the average grain sizes of the Al matrix were 10.6 and 12.3 μm in Figs. 10 (a) and (b), respectively, confirming that the grain size of the Al matrix does not vary regardless of the Fe content in the alloy. On the other hand, as was shown in Fig. 4, the amount and the size of the β phase particles vary with the Fe content significantly. Consequently, only the amount and the size of the β phase particles differed throughout the samples used in Fig. 9, and it was clarified that the β phase particles have a significant effect on the elongation of the present Al-Si-Fe alloys.

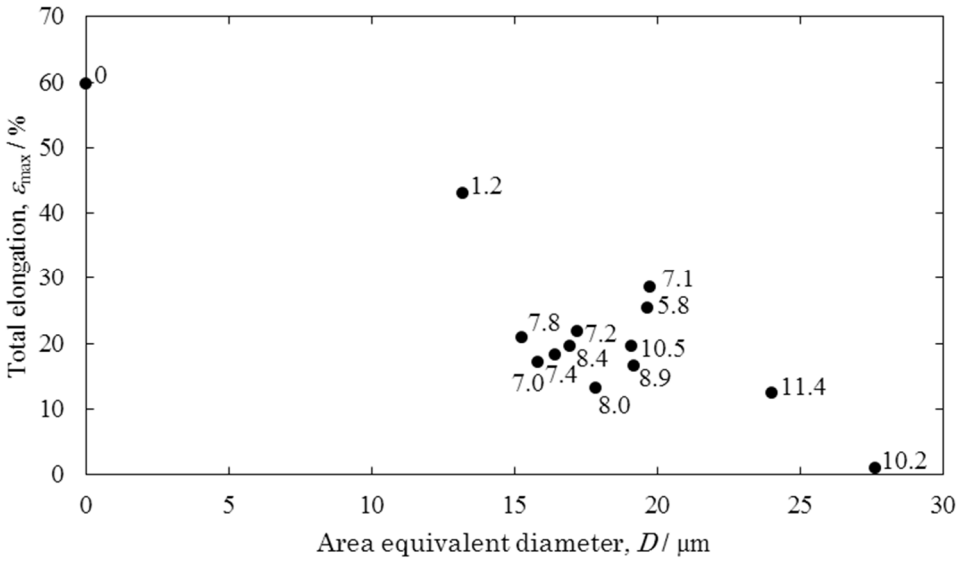

Fig. 9 The effect of area equivalent diameter of the β phase on the total elongation. The numbers on the plots are the volume fractions (%) of the intermetallic compound.

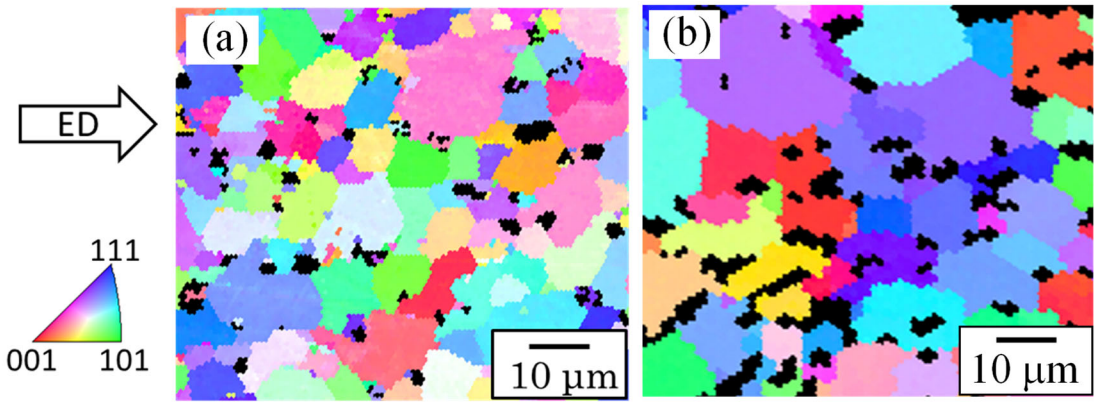

Fig. 10 Crystal orientation mapping of the Al matrix in the heteromorphic die extrudate of (a) Al-12Si-2Fe and (b) Al-12Si-4Fe alloys.

4.4 Rolling of the alloy

Samples taken from the as-cast billets and heteromorphic die extrudates were rolled by 77% at room temperature in 2 passes. In each pass, the thickness was reduced by 55%. The appearances of the rolled samples are shown in Fig. 11; (a) the as-cast billet containing 2 mass%Fe, (b) the heteromorphic die extrudate containing 2 mass%Fe, (c) the as-cast billet containing 4 mass%Fe, and (d) the heteromorphic die extrudate containing 4 mass%Fe. The rolling and the extrusion directions are transverse on the paper surface. In the case of the as-cast billet sample with 2 mass%Fe, although the targeted thickness was obtained by the two-pass rolling, the sample was torn into two parts in the width direction (Fig. 11 (a)). In the case of the as-cast billet sample with 4 mass%Fe, the rolled sample was fractured into two pieces in the longitudinal direction at the first pass (Fig. 11 (c)). The reason for such failure in billets is the presence of the brittle and coarse plate-like β phase particles. As indicated by the white arrows in Fig. 12, in the fracture part of the sample shown in Fig. 11 (c), cracks propagated along the longitudinal direction of the coarse plate-like β phase particles. Fig. 12 clearly demonstrates the consequences of the detrimental effect of the coarse β phase particles. On the contrary, in the heteromorphic die extrudates, the rolling was successfully achieved as shown in Figs. 11 (b) and (d). This is due to the refinement of the β phase particles by the heteromorphic die extrusion. It has been shown that the heteromorphic die extrusion can improve the ductility of the Al-Si alloys containing a large amount of Fe and allow them to undergo subsequent working processes such as cold rolling.

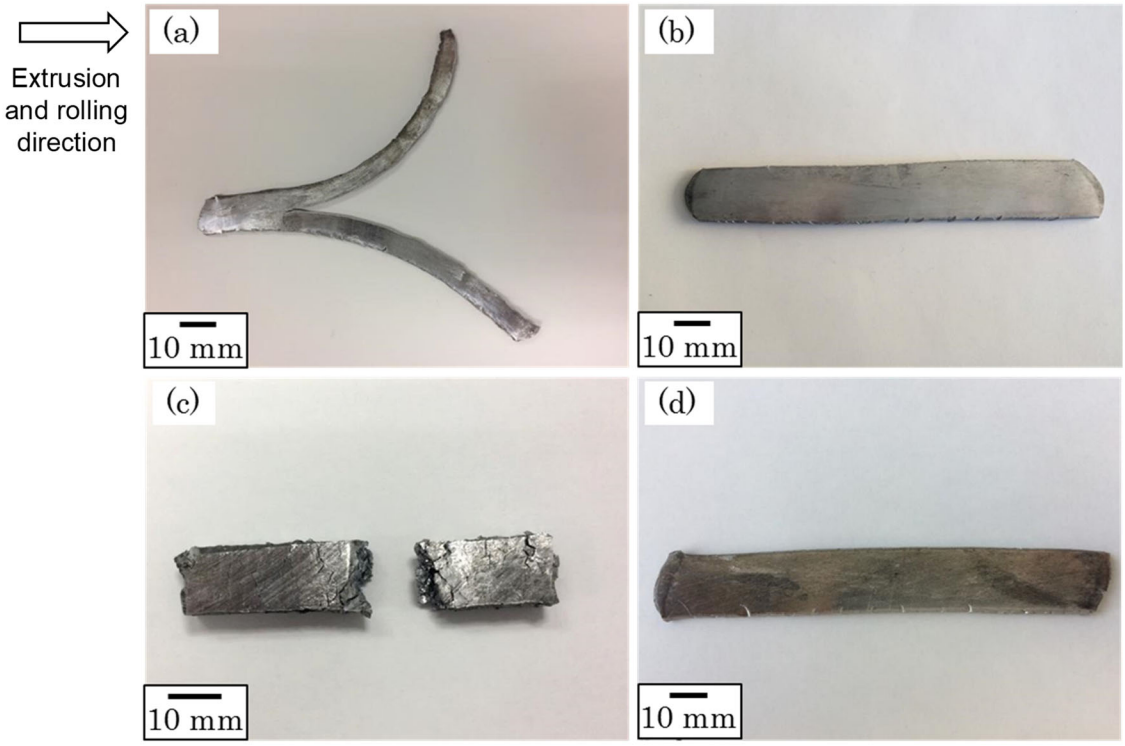

Fig. 11 Rolled samples of (a) as-cast billet containing 2 mass%Fe, (b) heteromorphic die extrudate containing 2 mass%Fe, (c) as-cast billet containing 4 mass%Fe and (d) heteromorphic die extrudate containing 4 mass%Fe.

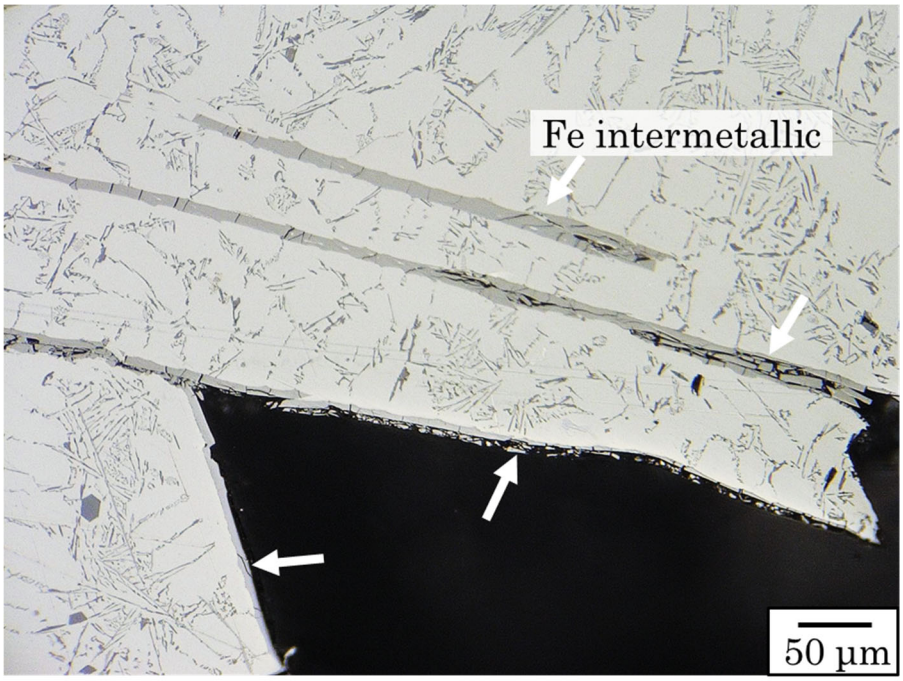

Fig. 12 Fracture part of the rolled sample shown in Fig. 11 (c).

4.5 Tensile test of the rolled sheet

Fig. 13 shows the tensile test results of the rolled samples in Fig. 11. Since it was not possible to obtain the tensile test specimen from the rolled billets, the results of the as-cast billets are shown instead in the figure for references. The measured elongations of the rolled samples obtained from the heteromorphic die extrudates with 2 and 4 mass%Fe were 39 and 18%, respectively. The elongations were almost the same as the ones of the extrudates shown in Fig. 7. The ultimate tensile strengths are 133 and 153 MPa in the rolled sheets with 2 and 4 mass%Fe, respectively. Compared with the strengths of the extrudates, the strength of the rolled sheet is slightly lower in the alloy with 2 mass%Fe, while slightly higher in the alloy with 4 mass%Fe. To investigate the reason for the change in the elongation and strength of the rolled sheet from the extrudate, microstructures of the Al-12Si alloys with 2 and 4 mass%Fe were observed and shown in Fig. 14. By the rolling process, the β phase particles were further refined, and their size was homogenized. In the rolled sheet with 2 mass%Fe, it can be considered that the changes of β phase particles by rolling process do not influence on the mechanical properties of the alloy much because the refining and homogenization in size distribution were fairly achieved in the as-extruded sample. In the case of the rolled sheet with 4 mass%Fe, there are cracks due to the fracture of the coarse β phase particles as indicated with the white arrows in Fig. 14 (b). It can be considered that this crack formation caused the slight deterioration in elongation of the rolled sheet with 4 mass%Fe. In both the extrudates and the rolled sheets, it can be said that there is no significant difference in the mechanical properties, and the both samples exhibited significant improvement in elongation and ultimate tensile strength compared with the as-cast billet. Therefore, it was found that the heteromorphic die extrusion gives a drastic improvement in plastic deformability, and Fe-containing Al-Si alloys can be used as a bar or sheet material by the extrusion of the ingot using the heteromorphic die.

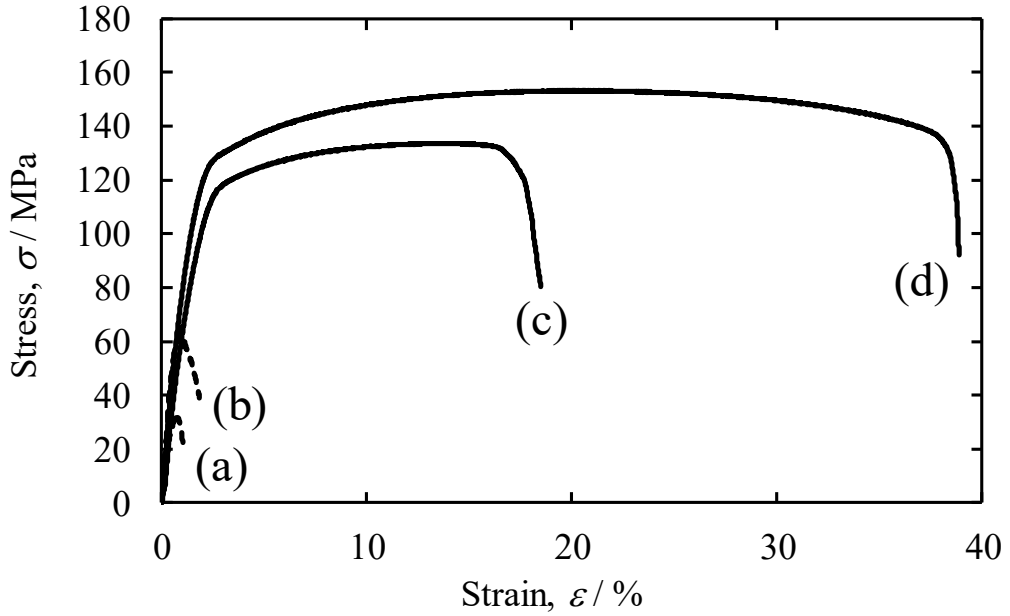

Fig. 13 Tensile test results of the rolled samples shown in Fig. 11; (a) as-cast billet containing 4 mass%Fe, (b) as-cast billet containing 2 mass%Fe, (c) heteromorphic die extrudate containing 4 mass%Fe, and (d) heteromorphic die extrudate containing 2 mass%Fe.

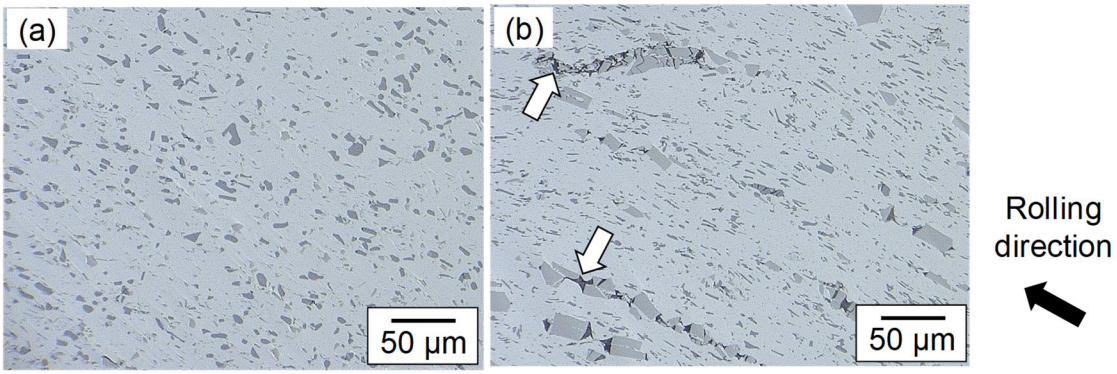

Fig. 14 Microstructures of the rolled sheet after heteromorphic die extrusion; (a) Al-12Si-2Fe alloy, and (b) Al-12Si-4Fe alloy.

5. Conclusions

Al-Si alloys containing a large amount of Fe were hot-extruded by using a specially designed heteromorphic die, and its effects on the refinement of the coarse and brittle intermetallic particles were investigated. The heteromorphic die has a significant effect on the refinement of the primary $Al_9Si_2Fe_2$ (β phase) particles and the eutectic Si particles. This is due to the large strain induced in the

billet metal at the right-angle corners of the die holes. The refinement of these particles is extremely effective for improving the ductility of the alloy. The extruded bar can be cold-rolled to produce a sheet, and the sheet has a good ductility. The present results imply that the Al-Si scraps with a high level of Fe concentration can be reused as a bar or sheet material by extrusion of the as-cast ingot using the present heteromorphic die.

Acknowledgements

The financial support by the Japan Aluminium Association is gratefully acknowledged. This work was partially supported by Nanotechnology Platform Program of the Ministry of Education, Culture, Sports, Science and Technology (MEXT), Japan. The authors are grateful to Prof. Maciej Pietrzyk and Mr. Stanisław Węglarczyk at AGH University of Science and Technology, Poland for their support in FE simulation.

References

Cai, Y., Liang, R., Hou, L., Zhang, J., 2011. Mater. Sci. Eng. A, 528, 4248-4254.

Chenot, J.-L., Bellet, M., 1992. The viscoplastic approach for the finite element modelling of metal forming processes. In: Hartley P, Pillinger I, Sturgess CEN (eds) Numerical modelling of material deformation processes, Springer-Verlag, London, pp. 179-224.

Das, S.K., Green, J.A.S., Kaufman, J.G., Emadi, D., Mahfoud, M., 2010. Aluminum recycling—An integrated, industrywide approach. JOM 62, 23-26.

Fang, L., Fuxiao, Y., Dazhi, Z., Liang, Z., 2011. Microstructure and mechanical properties of an Al–12.7Si–0.7Mg alloy processed by extrusion and heat treatment. Mater. Sci. Eng. A 528, 3786-3790.

Ham, G., Baek, M., Kin, J., Lee, S., Lee, K., 2017. Effect of heat treatment on tensile and fatigue deformation behavior of extruded Al-12 wt%Si alloy. Met. Mater. Int. 23, 35-42.

Khalifa, W., Tsunekawa, Y., Okumiya, M., 2010. Effect of ultrasonic treatment on the Fe-intermetallic phases in ADC12 die cast alloy. J. Mater. Process. Technol. 210, 2178-2187.

Mehtedi, M.El., Musharavati, F., Spigarelli, S., 2014. Modelling of the flow behaviour of wrought aluminium alloys at elevated temperatures by a new constitutive equation. Mater. Des. 54, 869-873.

Prusa, F., Vojtech, D., Blahova, M., Michalcova, A., Kubatik, T.F., Cizek, J., 2015. Mater. Des., 75, 65-75.

Fig. 1 Schematic drawing of heteromorphic die extrusion; (a) the overall setup, (b) strain-giving die and (c) shape-giving die.

Fig. 2 Schematic diagram of the tensile test specimen (dimensions in mm).

Fig. 3 The geometries of (a) the heteromorphic die extrusion and (b) the conventional die extrusion.

Fig. 4 Microstructures of (a) billet and (b) heteromorphic die extrudate containing 2 mass%Fe, and (c) billet and (d) heteromorphic die extrudate containing 4 mass%Fe. The white arrows in the figures indicate the β phase.

Fig. 5 (a) Cross section of strain-giving die and billet of Al-12mass%Si-4mass%Fe alloy. Figs (b) to (e): microstructures of the alloy in the positions indicated in (a). The white and black arrows indicate the β phase particles and the eutectic Si particles.

Fig. 6 Finite element simulation results of effective strain after (a) conventional die extrusion and (b) heteromorphic die extrusion processes. Figs. (c) and (d) represent enlargements of Figs (a) and (b), respectively.

Fig. 7 Tensile test results of (a) as-cast billet containing 4 mass%Fe, (b) as-cast billet containing 2 mass%Fe, (c) heteromorphic die extrudate containing 4 mass%Fe, and (d) heteromorphic die extrudate containing 2 mass%Fe.

Fig. 8 Fracture surface of (a) the billet and (b) the heteromorphic die extrudate containing 4 mass%Fe.

Fig. 9 The effect of area equivalent diameter of the β phase on the total elongation. The numbers on the plots are the volume fractions (%) of the intermetallic compound.

Fig. 10 Crystal orientation mapping of the Al matrix in the heteromorphic die extrudate of (a) Al-12Si-2Fe and (b) Al-12Si-4Fe alloys.

Fig. 11 Rolled samples of (a) as-cast billet containing 2 mass%Fe, (b) heteromorphic die extrudate containing 2 mass%Fe, (c) as-cast billet containing 4 mass%Fe and (d) heteromorphic die extrudate containing 4 mass%Fe.

Fig. 12 Fracture part of the rolled sample shown in Fig. 11 (c).

Fig. 13 Tensile test results of the rolled samples shown in Fig. 11; (a) as-cast billet containing 4 mass%Fe, (b) as-cast billet containing 2 mass%Fe, (c) heteromorphic die extrudate containing 4 mass%Fe, and (d) heteromorphic die extrudate containing 2 mass%Fe.

Fig. 14 Microstructures of the rolled sheet after heteromorphic die extrusion; (a) Al-12Si-2Fe alloy, and (b) Al-12Si-4Fe alloy.

Table 1 Effective strain values obtained from the simulation results after heteromorphic die and conventional die extrusion processes.